Original Article | *Peer Reviewed* | Open Access

Fusion of Wavelet Features and Gabor Features for SVM-based Iris Verification

Sayan Das* and Biswajit Kar

Check for updates

Department of Instrumentation Engineering, Central Institute of Technology Kokrajhar, Assam-783370, India

E-mail/Orcid Id:

SD, ✉ sayan.eie@gmail.com, 🆔 https://orcid.org/0009-0006-4644-9438;

BK, ✉ b.kar@cit.ac.in, 🆔 https://orcid.org/0000-0003-2686-5814

Abstract: Iris verification now become increasingly prominent in biometric-based person verification systems. It has gained a significant role in biometric systems due to its stability, high uniqueness, contactless and non-invasive properties. Iris has more inherent distinctive features than other biometrics. Feature extraction of iris plays a crucial role in this system for accurate person verification. Using the feature extraction process, unique iris features like textural patterns, crypts, and furrows of iris are extracted. In our study, we did a fusion of Discrete Wavelet Transform (DWT) features with multiple wavelet bases (db4, haar, coif3, and sym4) and Gabor features, which contain a good amount of textural and localized information. Fusion here indicates the concatenation of the extracted features using the above techniques. In this work, we studied this method on the full iris only so that a maximum number of features can be extracted. This combined approach yielded a significant 112 number of features. The extracted features are then verified using a support vector machine (SVM) classifier based on radial basis function (RBF) kernel with training vs testing split ratios of 8:2, 6:4, 4:6 and 2:8. In this study, we achieved the highest overall verification accuracy of 95.9% with training vs testing split ratio of 8:2. For other training vs testing split ratios of 6:4, 4:6 and 2:8 we achieved overall verification accuracies of 91.4%, 93.2% and 91.2% respectively. We got an overall verification accuracy of 92.9%, considering training vs testing ratios of 8:2, 6:4, 4:6 and 2:8.

Introduction

In the biometric verification process, the iris plays a significant role (Vacca, 2007). The iris has the distinct and most variable structure of the iris pattern between different individuals. Iris remains remarkably stable throughout a person's lifetime. So, it proves advantageous among the other human body parts. It is protected by the eyelids. So, it is safe from environmental factors. These are the main reasons for its exceptional reliability, accuracy, and performance compared to other biometric verification methods. Dhage et al. (2015) introduced an approach where they used DWT (Discrete wavelet transform) with DCT (Discrete cosine transform) for iris feature extraction. They used the haar wavelet as the mother wavelet function within the DWT stage and then added the DCT features to them. They worked on the IITD iris database and achieved a recognition rate of 90.59%. Thakkar and Patel (2020) Extracted the Gabor

features. They used a supervised neural network. The authors trained the NN (Neural Network) with 80% of the irises. Working on CASIA V4 datasets authors achieved an accuracy of 99.99% (Kranthi Kumar et al., 2021) in their work compared two approaches. In their work, they used CNN (Convolutional Neural Network) and Gabor filter for feature extraction. Then they used SVM (Support Vector Machine) and NN for the classification. They worked with CASIA V1 datasets and claimed CNN with NN achieved better accuracy. El-Sayed and Abdel-Latif (2022) in their work extracted Gabor features and DWT features. The authors used a multi-class SVM classifier. They worked on IITD datasets, extracted 88 features and found 98.92% accuracy. Das and Kar (2022) surveyed the current iris verification systems. The authors highlighted the challenges in different steps in the process of iris verification. Most of the existing systems do not work well due to noise like eyelids, eyelashes,

reflections, blurriness due to subject movement etc. Feature selection in the domain of biometric verification was investigated by (Chetry and Kar, 2024; Dixit et al., 2024). They have used Kruskal Wallis and mRMR techniques in online signature verification procedure using the SVM and KNN classifier. El-Sofany et al. (2024) worked on improving cloud security using the iris recognition technique. They have used a hybrid approach for feature extraction and classification using Hamming distance and convolutional neural network for iris recognition. They worked on datasets (MMU, IITD and CASIA) and achieved good recognition rates (99.5%, CASIA databases. Hence, we choose this database to work on. For our work, we sorted the iris of the persons whose all five irises are free from noise. This is done in the preprocessing stage of our work. After sorting the database the number of irises reduced to 305. So, we choose the SVM classifier for iris verification. SVM is then trained and verified with the training vs testing ratios of 8:2, 6:4, 4:6 and 2:8.

Materials and Methods
Block diagram of the proposed method

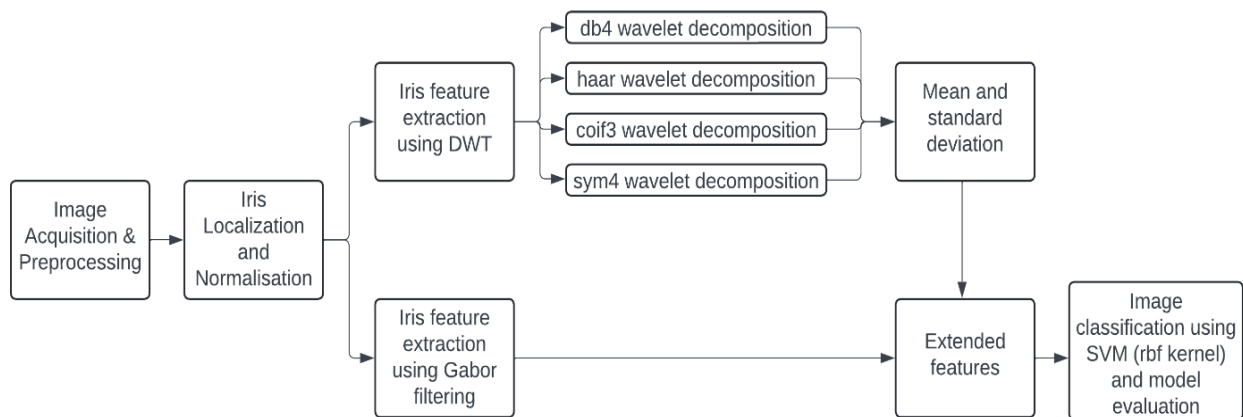The block diagram of the overall proposed system is

Figure 1. Block diagram.

97.2% and 95%). Chen et al. (2023) did a comparison study among the CNN algorithm and improved PCHIP-LMD algorithm. They found that CNN achieves a higher correct recognition rate (92%) compared to the PCHIP-LMD algorithm (78%) for a larger dataset. Madanan et al. (2023) have done a comparative study between SVM and CNN for image classification. They found that on smaller datasets SVM performs better than CNN (85% vs. 82%). Gautam et al. (2022) used supervised and deep learning classifiers for detecting and classifying brain tumours using MRI images. They used SVM, decision tree, Naïve Bayes and Linear regression for the binary classification and achieved the highest accuracy of 96% with SVM and decision tree.

Our research work proposes an iris feature extraction approach that combines multi-wavelet features with Gabor features. We do a fusion of these two features to accumulate a larger number of features and verify a person with the same. Our method aims to capture a comprehensive set of iris features for stricter recognition during iris verification. In this work, we worked with the images from the UBIRIS V1.0 database. We found that most of the previous works were done on the IITD and shown in Figure 1.

In this diagram, it has been shown that first the image acquisition is done and pre-processed. Then the iris is localised from the image, segmented, extracted and normalised. Then the normalised iris is fed to the feature extraction module. The extracted feature is then classified using the SVM. The detailed method is discussed in the following sections.

Image acquisition and preprocessing

Image preprocessing is a crucial step in iris verification systems (Nazmdeh et al., 2019). It aims to prepare the captured iris image for subsequent segmentation and feature extraction stages. Here common preprocessing techniques (Fathee and Sahmoud, 2021) have been used.

Image acquisition

In this experimental work, the UBIRIS V.1 (200×150 Grayscale) (Proença and Alexandre, 2005) iris database is used. In this mentioned database the images were captured using a Nikon E5700 camera in RGB colour format with a focal length of 71 millimetres at a shutter speed of 1/30 of a second and an ISO speed of 200. Some of the sample images are shown in Figure 2.
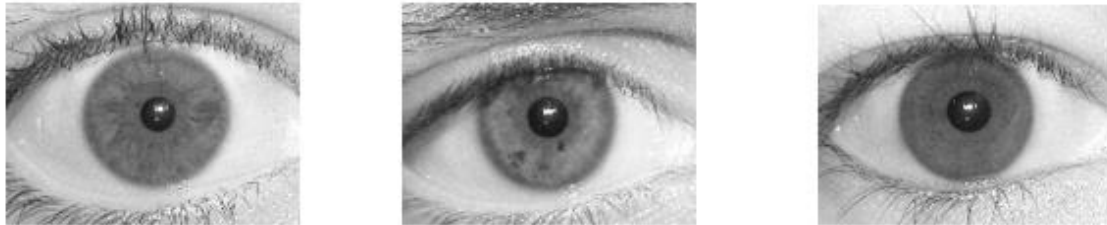
Figure 2. Sample iris images.

Noise reduction and Canny edge detection

In this work for noise reduction, a median blur filter of window size of 5×5 has been applied (Jamaludin et al., 2021). The median blur filter smooths the iris images by replacing each pixel with the median value of its surrounding neighbourhood. Unlike averaging which can blur edges, the median filter prioritizes values present in the image, making it great for preserving sharp details while cleaning up noisy areas.

Then, the Canny edge detection (Canny, 1986) is applied to the de-noised image for accurate edge identification. Canny edge detection excels at finding crisp edges in images. It employs a multi-step process: first, a Gaussian filter smoothing the image to reduce noise shown in Equation 1.

$$G(m,n) = \frac{1}{2\Pi\sigma^2} e^{-\frac{(m^2+n^2)}{2\sigma^2}} \dots\dots\dots\dots\dots\dots\dots .(1)$$

Then, gradients (intensity changes) are calculated using Sobel filters (Vishwakarma and Patel, 2019) to find the direction and magnitude of the strongest intensity change. ($|G_m| + |G_n|$). Non-maximum suppression thins edge to single pixels, and finally, double thresholding (with hysteresis) ensures only strong edges and their connected weaker neighbours are kept.

Iris Localization

This step involves identifying the iris region within the captured eye image. Here the Hough transform for circle detection (Illingworth and Kittler, 1987) is applied to detect the pupil and the iris boundary.

Circles in 2D images can be described by their centre (m, n) and radius (r) (Equation 2). We can find these parameters by considering the equation

$$(x-m)^2 + (y-n)^2 = r^2 \dots\dots\dots\dots\dots\dots\dots\dots (2)$$

This translates to a 3D parameter space where each point represents a possible circle (centre and radius). Finding circles becomes identifying the intersection of many "cones" in this space, each cone originating from a fixed point (x, y) on the image. It can be achieved in two steps:
1. Fix the radius and search for the best centre in a 2D space.
2. Find the optimal radius by searching a 1D space.

Iris Segmentation

Once the iris region is localized, its inner and outer boundary perimeters are calculated. Then the small circle i.e., the pupil area and the area beyond the outer boundary perimeters are masked. The donut-shaped iris is then extracted from the iris image (Roy and Soni, 2016).

Normalisation

To normalise the iris image for further processing the Daugman's Rubber Sheet Model (Daugman, 1993) is used. This model normalizes iris images by warping them into a polar grid. This removes the influence of pupil size and other variations, focusing on the iris pattern itself.
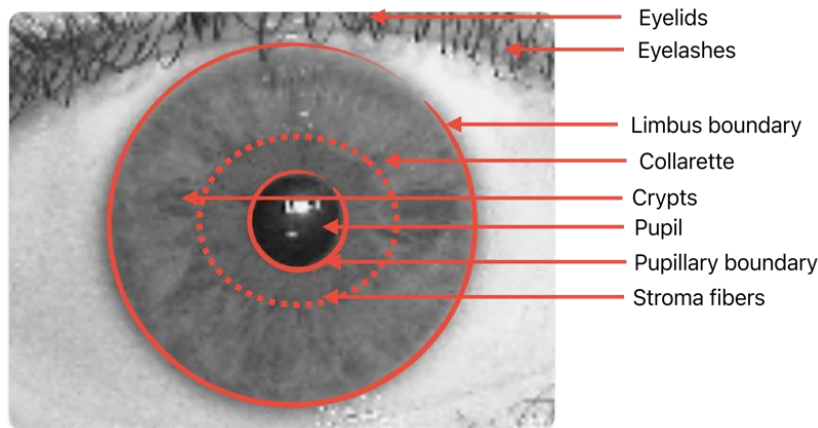

Figure 3. Features of an iris.

The model achieves this by converting each point in the iris region from rectangular coordinates (m, n) to a normalized polar representation. So, the original iris image in raw coordinates (m, n) can be transformed into a normalized polar coordinate system (r, θ) using the following model shown in Equation 3.

$$IR\big(m(r,\theta), n(r,\theta)\big) \rightarrow IR(r,\theta) \ldots \ldots \ldots \ldots \ldots \ldots (3)$$

Feature Extraction

Iris features (Edwards et al., 2016) refer to the unique patterns and textures present within the iris shown in Figure 3.

Types of Iris Features

Stroma: The stroma (Treuting et al., 2012) is the loose connective tissue layer that forms the bulk of the iris. It contains pigment cells (melanocytes) that determine eye colour. Variations in these pigment cells' density and distribution contribute to the iris' unique patterns.

Crypts: These are small, pit-like structures on the iris surface (Chua et al., 2016). Their size, shape, and distribution vary considerably between individuals.

Furrows: Furrows (Larsson et al., 2011) are ridges or folds on the iris surface. Similar to crypts, their characteristics contribute to the overall iris pattern.

Collagenous fibres: These microscopic fibres form a network within the stroma, influencing the iris texture (Rittig et al., 1990).

Lacunae: Lacunae (Shen et al., 2007) are small holes or gaps within the iris stroma. Their presence and arrangement add to the unique details of the iris.

In this experimental work, two feature extraction methods have been applied combined to achieve a good number of features which has been discussed in the following section.

Discrete Wavelet Transform

The pre-processed iris image is decomposed using a 2-D DWT (Wei et al., 2005). This breaks down the image into different frequency subbands (approximation and detail), capturing features at various scales.

The DWT (Hosseinzadeh, 2020) may defined as:

$$D_\varphi(j_0, k) = \frac{1}{\sqrt{V}} \sum_x f(m)\varphi_{j_0,k}(m) \ldots \ldots \ldots \ldots \ldots (4)$$

$$D_\psi(j_0, k) = \frac{1}{\sqrt{V}} \sum_k f(m)\psi_{j_0,k}(m) \ldots \ldots \ldots \ldots \ldots (5)$$

where $f(m)$, $\varphi_{j_0,k}(m)$, and $\psi_{j,k}(m)$ are functions of the discrete variable $m = 0,1,2,\ldots,(V-1)$.

2-D DWT provides a multi-resolution representation of the iris, potentially capturing both global (low-frequency) and local (high-frequency) features. Specific subbands or coefficients within the DWT decomposition are chosen to represent the iris features. These features might capture textural patterns, edge information, or specific frequency components relevant to iris identification. In this work, the study has been performed by the multiple features extracted using Daubechies 4 wavelet, Haar wavelet, coiflet 3 wavelet and Symlet 4 wavelet.

The db4 wavelet, also known as the Daubechies 4 wavelet (Lindfield and Penny, 2019), is a specific type of wavelet function used in wavelet transforms. It has 4 vanishing moments, which means it can effectively represent signals with up to a cubic polynomial trend (constant, linear, and quadratic terms). The db4 function has a finite duration, meaning it's zero outside a specific range. This allows for efficient analysis of localized features in a signal. 4 Vanishing Moments property makes it suitable for representing signals that don't have strong low-frequency components or trends.

The scaling and wavelet functions (Jensen and la Cour-Harbo, 2001) are given in the following equations:

Scaling function:

$$f_i = d_0 s_{2i} + d_1 s_{2i+1} + d_2 s_{2i+2} + d_3 s_{2i+3} \ldots \ldots \ldots (6)$$

Wavelet function:

$$w_i = c_0 s_{2i} + c_1 s_{2i+1} + c_2 s_{2i+2} + c_3 s_{2i+3} \ldots \ldots \ldots (7)$$

Haar wavelets (Aboufadel and Schlicker, 2003) are very basic and computationally inexpensive to apply compared to other wavelets used here as a preliminary feature extraction step to identify basic edges and eliminate irrelevant image regions.

Haar functions (Hariharan and Kannan, 2014) can be expressed as:

$$Z_i(t) = \begin{cases} 1, & for\ t \in \frac{m}{l}, \frac{m+0.5}{l} \\ -1, & for\ t \in \frac{m+0.5}{l}, \frac{m+1}{l} \\ 0, & elsewhere \end{cases} \ldots \ldots \ldots \ldots \ldots (8)$$

$l = 2^n (n = 0,1,2 \ldots N)$ points wavelet level and translation parameter $m = 0,1,2,\ldots l-1$.

The *coiflet 3 wavelet* has a finite duration, allowing for the analysis of localized features in the iris image. It has 3 vanishing moments, which means it can effectively represent signals with up to quadratic polynomial trends (constant and linear terms).

Mathematically, it can be represented as (Daubechies, 1999)-

$$C_i = (-1)^i S_{N-1-i} \ldots \ldots \ldots \ldots \ldots \ldots \ldots \ldots \ldots (9)$$

Where i is the coefficient index, C is a wavelet coefficient, S is a scaling function coefficient and N is the wavelet index.

The *symlet 4 wavelets* (Bahri et al., 2018), in short, sym4 wavelets have a finite duration, allowing for analysis of localized features in the iris image, well known for their near-symmetry feature extraction

algorithm. This wavelet is based on the Daubechies wavelet but is modified to have near-symmetrical properties. The higher the 'order' of this wavelet, the greater the symmetry becomes.

Gabor filters and iris textures

Using the Gabor filter at different orientations and scales, a rich feature representation of the iris texture can be obtained. The features extracted by Gabor filters effectively differentiate between different irises. In this work, a bank of Gabor filters with various orientations and frequencies is applied to the pre-processed iris image. This creates multiple filtered images highlighting features at different scales and orientations. These filters can be defined by the following expression (Shen et al., 2007)

$$\psi(m,n) = \frac{f_u^2}{\pi k \eta} e^{\left(\frac{f_u^2}{k^2}\right)m'^2 + \left(\frac{f_u^2}{\eta^2}\right)n'^2} e^{j2\pi f_u m^2} \dots\dots (10)$$

where, $m' = m\cos\theta_v + n\sin\theta_v$,
$n' = -m\sin\theta_v + n\cos\theta_v$,
$f_u = \frac{f_{max}}{2^{\left(\frac{u}{2}\right)}}$,
$\theta_v = \frac{v\pi}{8}$

Here, η is the ratio between the centre frequency and the Gaussian envelope size, and θ_v and f_u represents the orientation and center frequency, respectively.

Features are first extracted using the discrete wavelet transform using the mentioned wavelet techniques i.e., db4, haar, coif3 and sym 4 from the normalised iris images. This process involves statistical measures like mean and standard deviation within specific regions of the filtered images. Specific subbands or coefficients within the DWT decomposition are chosen to represent the iris features which capture the textural patterns, edge information, and specific frequency components relevant for iris verification. Then, the same normalised image is processed using the Gabor kernel to extract more features.

Feature Vector Formation: The extracted features using the mentioned two methods are then combined to form a feature vector that represents the iris.

Iris template generation

This work utilizes a database containing five iris samples for each individual. To identify the most suitable iris image for recognition purposes, the following method is applied:

Mean Feature Calculation: The average values for all the extracted iris features are first calculated across all five samples belonging to the same person.

Euclidean Distance Measurement (Xu et al., 2020): In the next stage, each iris image is compared to this mean feature vector. The Euclidean distance, a measure of similarity, is calculated between the feature vector of each image and the mean vector using the following formula:

Let point b have cartesian coordinates (b_1, b_2), and let point c have coordinates (c_1, c_2). Then, the distance between b and c may expressed as (Cohen et al., 2005)

$$d(b,c) = \sqrt{(b_1 - c_1)^2 + (b_2 - c_2)^2} \dots\dots\dots(11)$$

Template Selection: The iris image that produces the smallest Euclidean distance from the mean feature vector is chosen as the best representative. This image will then be used as the iris template for that specific person for further recognition tasks.

This process ensures that the chosen iris template accurately reflects the typical features present within an individual's iris, improving the overall recognition accuracy.

Support Vector Machines (SVM)

Support Vector Machine (SVM) (Sesmero et al., 2021) finds an optimal hyperplane in a high-dimensional space. The data points of different classes with the maximum margin can be separated using this classifier. Here, the margin indicates the distance between the hyperplane and the support vectors, the closest data points of each class. SVMs are supervised learning algorithms. So, in that case, each data point has to be a corresponding class label. SVM learns and classifies them.

Assuming a set of data points, let's say there are n of them and each point is like a location with coordinates $(x_1, y_1), (x_2, y_2)....(x_n, y_n)$ (Cortes et al., 1995). These points can belong to two different groups, represented by y_i, either a 1 or a -1, each indicating the class to which the point x_i belongs. The x_i can be thought of as a p-dimensional real vector. To find a hyperplane in higher dimensions that best separates the points belonging to group $y_i = 1$ from those belonging to group $y_i = -1$. This line should be positioned in a way that maximizes the distance between the line and the closest points from each group. Imagine a margin of separation, and we want to make that margin as wide as possible.

Any line (or hyperplane in higher dimensions) can be described by an equation. Here, we use the equation 12.

$$w^T m - a = 0 \dots\dots\dots\dots\dots\dots(12)$$

w is a vector representing the direction perpendicular to the line, m is any point in the data set, a is a value that determines how far the line is positioned away from the origin (0,0) along the direction of w. The value $\frac{a}{\|w\|}$ (where $\|w\|$ represents the length of w) tells us how far the line is from the origin along the direction of w.

RBF (Radial Basis Function)

SVMs normally work on linear data. But it can handle non-linear data too by using a kernel function. The RBF (Radial Basis Function) (Chen and Bakshi, 2009) kernel is a popular choice for use with Support Vector Machines (SVMs) when dealing with non-linear data. The Radial basis function is a kernel to handle non-linear data. Here, γ decides the width of the kernel and also the model complexity. The function is expressed in the equation 13.

$$R(m,n) = exp\left(-\gamma \|m - n\|^2\right) \dots \dots \dots \dots \dots (13)$$

The flowchart of the proposed system is shown in Figure 4.

Results and Discussion

In this experimental work, we choose the UBIRIS V.1 database because all iris image sizes in this database are 150×200 pixels in grayscale. As we are using SVM as a classifier in the verification process, the small image size and depth help with faster processing. In this database, the total number of individuals is 239. For each person,

following sample image shows how an image is loaded for preprocessing (Figure 5).

The image is de-noise using a median blur filter of window size 5×5. Then, the canny edge detection algorithm is applied to it with σ value of 3, low threshold and high threshold value of 10 and 50, respectively.

After preprocessing, the pupil and iris boundary is detected using Hough transform for circle detection. Figure 6 shows two green colour circle perimeters detected using the mentioned technique.

The Iris pupil and the area beyond the iris perimeter are masked. After masking, only the donut-shaped iris remains. Figure 7 shows the result after masking.

As mentioned in Materials and Methods, in this experimental work the features are extracted using second-level discrete wavelet transform of four wavelets i.e., db4, haar, coif3 and sym4.

Using this algorithm, 16 numbers of features are generated. We wanted to work with a larger number of features. So, we extracted the Gabor features, a total of
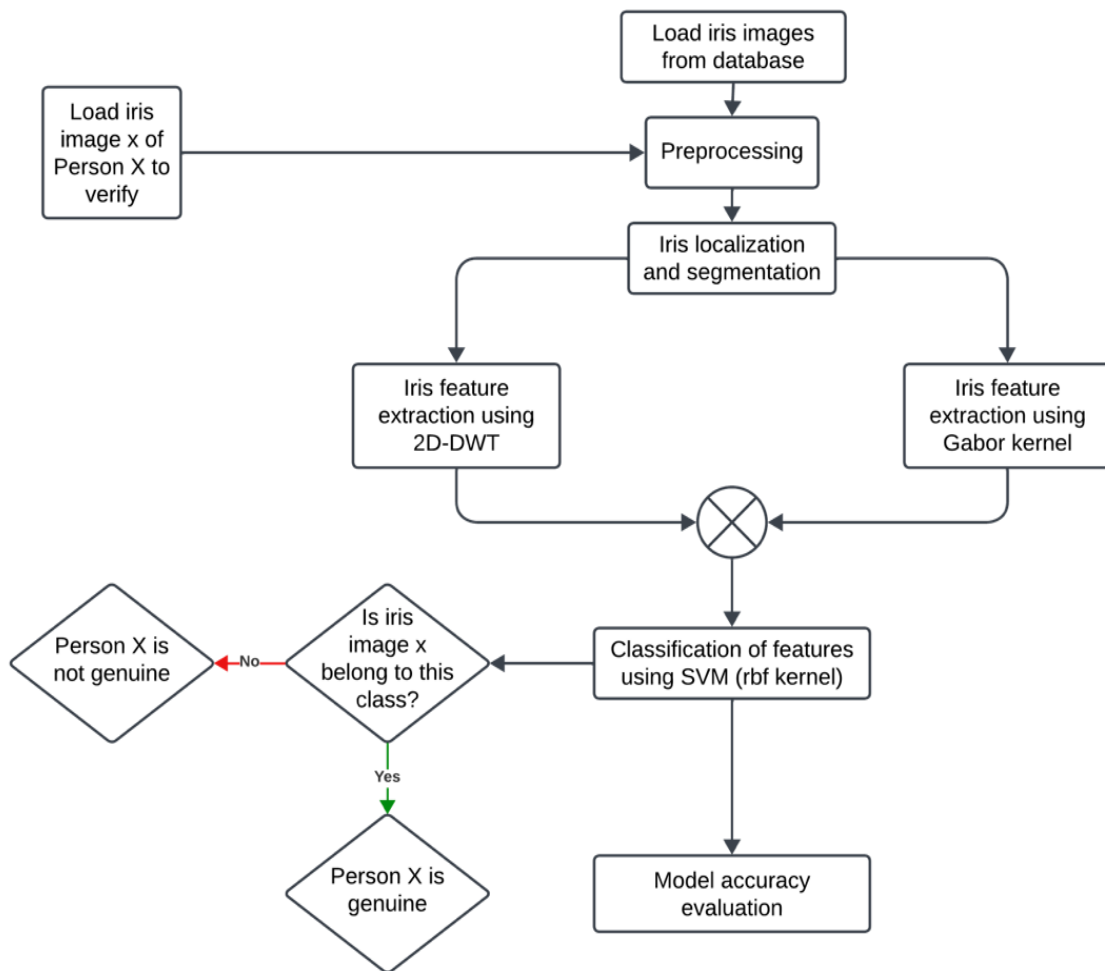

Figure 4. Flowchart of the overall system.

five iris images are available. The entire code is developed in the Python 3 compute engine. The

96 in numbers. Then, we fusioned extracted features using both methods, which resulted in a total of 112

features in the count. The feature vector size for a single image is 7168 bits. For 5 images for one individual, the feature size becomes 35840 bits.
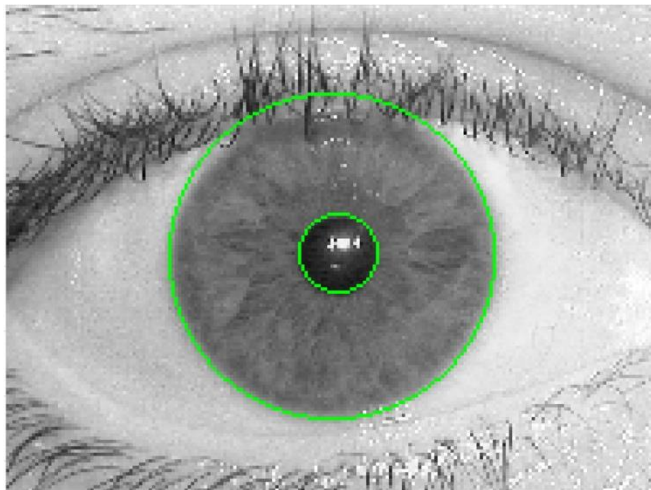

Figure 5. Loaded sample iris image.

Figure 6. Iris and pupil boundary detection.

Subjects are also arranged in an array where each element corresponds to the label for the respective sample in the features data.

Splitting data into training and testing sets is essential for unbiased evaluation of a machine learning model's performance. The training set is used to train the model, and the testing set is used to assess how well the trained model generalizes to unseen data.

In our work, we applied very strict criteria for circle detection for iris segmentation. Out of 239 persons' irises, we only consider those persons whose full iris can be extracted from the five iris images for the same individual. Rest images have some noises like eye occlusion due to eyelashes and eyelids, blurriness, close pigmentation of iris and pupil etc. Using this approach, we got 61 person irises, whose full iris was successfully extracted from the 5 images of each individual. In our work, after preprocessing, we reorganized the person IDs obtained from the UBIRIS database into a sequential order for easier management and analysis.

In Table 1, we show the verification accuracy for the 61 persons. Here we used SVM for the verification. To measure the verification accuracy we took 5 irises from each of two consecutive persons. Now, the model has 10 irises of two persons to be tested upon. We then split the training set and testing set into the following ratios 8:2, 6:4, 4:6 and 2:8. We do this same process for 61 persons. After calculating the overall accuracy we found that for training vs testing split ratio of 8:2, the verification accuracy is 95.9%. The overall accuracy using this model for four types of training vs testing split ratios is 92.9%. In Table 1 person verification accuracy for training : testing split ratios of 8:2, 6:4, 4:6, 2:8 and their overall
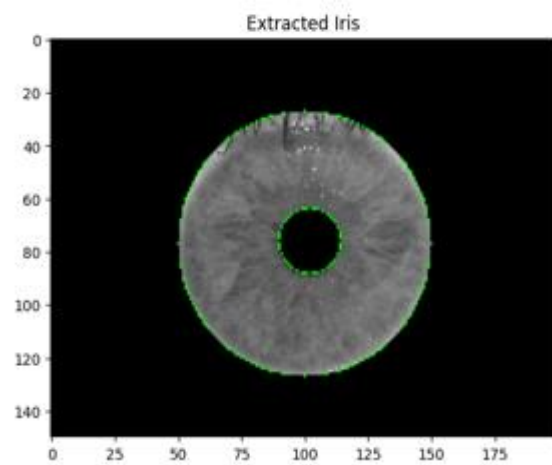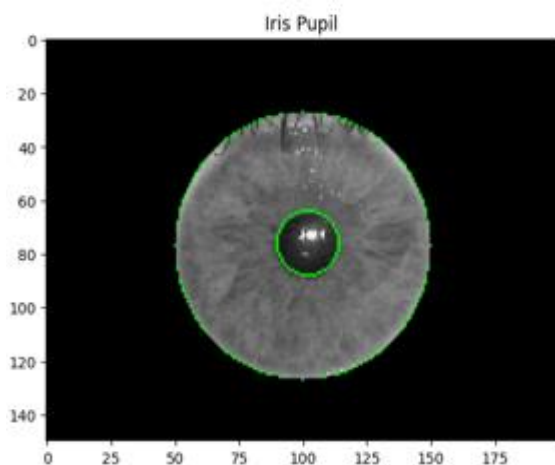

Figure 7. The masked area beyond the iris and pupil.

Feature data is arranged in a 2D array such that each row represents a sample (data point) and each column represents a feature.

accuracy has been shown.

Table 1. Verification accuracy for different training/testing sets of the person's irises.

Person ID	Training: Testing data ratio for verification accuracy measurement				Subject-wise Overall Accuracy
	8:2 (%)	6:4 (%)	4:6 (%)	2:8 (%)	Individual Accuracy (%)
1	100	100	100	100	100.0
2	100	100	100	88	96.9
3	100	75	100	88	90.6
4	100	100	100	100	100.0
5	100	100	100	100	100.0
6	100	100	100	100	100.0
7	100	100	100	100	100.0
8	100	100	100	100	100.0
9	100	100	100	100	100.0
10	100	100	100	100	100.0
11	100	100	100	100	100.0
12	100	100	100	100	100.0
13	100	100	100	100	100.0
14	100	100	100	100	100.0
15	100	75	83	88	86.5
16	100	100	100	100	100.0
17	100	100	100	100	100.0
18	50	50	50	50	50.0
19	50	50	50	50	50.0
20	100	100	100	100	100.0
21	100	100	100	100	100.0
22	50	50	67	63	57.3
23	100	100	100	100	100.0
24	100	100	100	100	100.0
25	100	100	83	88	92.7
26	100	100	100	100	100.0
27	100	100	100	100	100.0
28	100	100	100	100	100.0
29	100	50	67	63	69.8
30	100	100	100	100	100.0
31	100	100	100	100	100.0
32	100	100	100	100	100.0
33	100	100	100	100	100.0
34	100	75	100	100	93.8
35	100	100	100	100	100.0
36	100	100	100	100	100.0
37	50	50	67	63	57.3
38	100	100	100	100	100.0
39	100	100	100	100	100.0
40	100	100	100	100	100.0
41	100	100	100	100	100.0
42	100	100	100	100	100.0

43	50	100	100	100	87.5
44	100	25	83	88	74.0
45	100	100	83	88	92.7
46	100	100	100	100	100.0
47	100	75	83	0	64.6
48	100	100	50	38	71.9
49	100	75	83	75	83.3
50	100	100	100	100	100.0
51	100	100	100	100	100.0
52	100	100	100	100	100.0
53	100	100	100	88	96.9
54	100	100	100	75	93.8
55	100	100	100	100	100.0
56	100	50	50	100	75.0
57	100	100	83	88	92.7
58	100	100	100	100	100.0
59	100	100	100	100	100.0
60	100	75	100	88	90.6
61	100	100	100	100	100.0
Training: Testing ratio-wise overall accuracy					
Overall Accuracy (%)	**95.9**	91.4	93.2	91.2	92.9

As per the result achieved, shown in Table 1 we calculated the person verification accuracy. In Figure 8 individual person-wise overall accuracy is shown for the model used.

In Figure 9 the average verification accuracy has been compared for training vs testing split ratios of 8:2, 6:4, 4:6 and 2:8.

From these results, it has been observed that by combining the extracted features using DWT and Gabor we got 112 features. During verification, we are verifying all those features for the person to be verified. The highest accuracy we achieved using the supervised machine learning technique was 95.9%, where we trained the model using 80% of a single person's features. When this model is trained with only 20% of a single person's features, we achieved a verification accuracy of 91.2%.

Conclusion

In our work, we first extracted the iris from the image after preprocessing. The work is performed only on the full iris. So, we considered those person's irises whose all five irises are free from noise. We normalised it and did a fusion of wavelet features and Gabor features. This combination led to a significant 112 number of features capturing various aspects of the iris. We then used SVM with RBF kernel for verification of the 61 persons we considered. The best verification accuracy achieved is 95.9% with a training vs testing split ratio of 8:2. We achieved an average verification accuracy of 92.9% on training vs testing split ratios of 8:2, 6:4, 4:6 and 2:8. Here we used cloud-based Python 3 Google compute engine to compile our work. However, the large number of features might compromise processing speed. Future work will explore feature selection techniques to enhance the system's efficiency while maintaining accuracy. As well as we will also focus on the preprocessing so that instead of performing verification with full iris only. The noise-free areas of the iris can be considered for verification. So the data size will increase and there is a possibility that for each person we may not get five irises due to noise. Hence, we have to use deep learning techniques like convolutional neural networks (CNN) for training and verification purposes.

Acknowledgement

Figure 8. Person-wise verification accuracy chart.

Figure 9. Training : testing ratio vs average verification accuracy.

Conflict of Interest

The authors declare no conflict of interest.

References

Aboufadel, E., & Schlicker, S. (2003). Wavelets, Introduction. In *Elsevier eBooks*, pp. 773–788. https://doi.org/10.1016/b0-12-227410-5/00823-1

Bahri, S., Awalushaumi, L., & Susanto, M. (2018). The Approximation of Nonlinear Function using Daubechies and Symlets Wavelets. In *Proceedings of the International Conference on Mathematics and Islam (ICMIs 2018),* pp. 300-306. https://doi.org/10.5220/0008521103000306

Canny, J. (1986). A computational approach to edge detection. *IEEE Transactions on Pattern Analysis and Machine Intelligence*, *PAMI-8*(6), 679–698. https://doi.org/10.1109/tpami.1986.4767851

Chen, H., & Bakshi, B. (2009). Linear approaches for nonlinear modeling. In *Elsevier eBooks,* pp. 453–462. https://doi.org/10.1016/b978-044452701-1.00060-0

Chen, Y., Zhao, Y., Zhao, B., & Wei, H. (2023). Research on Iris feature extraction and recognition technology based on deep learning. *International Journal of Advanced Network Monitoring and Controls*, *8*(3), 35–45. https://doi.org/10.2478/ijanmc-2023-0064

Chetry, B. P., & Kar, B. (2024). Kruskal Wallis and mRMR Feature Selection based Online Signature Verification System using Multiple SVM and KNN. *International Journal of Experimental Research and Review*, *42*, 298–311. https://doi.org/10.52756/ijerr.2024.v42.026

Chua, J., Thakku, S. G., Tun, T. A., Nongpiur, M. E., Tan, M. C. L., Girard, M. J., Wong, T. Y., Quah, J. H. M., Aung, T., & Cheng, C. (2016). Iris crypts influence dynamic changes of iris volume. *Ophthalmology*, *123*(10), 2077–2084. https://doi.org/10.1016/j.ophtha.2016.06.034

Cohen, David., Lee, Theodore., & Sklar, David. (2005). *Precalculus : a problems-oriented approach*. https://books.google.com/books/about/Precalculus_A_Problems_Oriented_Approach.html?id=_6ukev29gmgC

Cortes, C., & Vapnik, V. (1995). Support-vector networks. *Machine Learning*, *20*(3), 273–297. https://doi.org/10.1007/bf00994018

Das, S., & Kar, B. (2022). Verification of Iris with Consideration of Constraints. In Sharma, H.,

Shrivastava, V., Bharti, K. K. & Wang, L. (Eds.), *Proceedings of the International Conference on Communication and Intelligent Systems (ICCIS 2021), Lecture Notes in Networks and Systems, 461,* 95–106. https://doi.org/10.1007/978-981-19-2130-8_8

Daubechies, I. (1992). Ten lectures on wavelets, Society for Industrial and Applied Mathematics, 3600 University City Science Center Philadelphia, PA, USA, ISBN:978-0-89871-274-2

Daugman, J. (1993). High confidence visual recognition of persons by a test of statistical independence. *IEEE Transactions on Pattern Analysis and Machine Intelligence*, *15*(11), 1148–1161. https://doi.org/10.1109/34.244676

Dhage, S. S., Hegde, S. S., Manikantan, K., & Ramachandran, S. (2015). DWT-based feature extraction and Radon Transform based contrast enhancement for improved iris recognition. *Procedia Computer Science*, *45*, 256–265. https://doi.org/10.1016/j.procs.2015.03.135

Dixit, A., Gupta, A., Chaplot, N., & Bharti, V. (2024). Emoji Support Predictive Mental Health Assessment Using Machine Learning: Unveiling Personalized Intervention Avenues. *International Journal of Experimental Research and Review*, *42*, 228-240. https://doi.org/10.52756/ijerr.2024.v42.020

Edwards, M., Cha, D., Krithika, S., Johnson, M., & Parra, E. J. (2016). Analysis of iris surface features in populations of diverse ancestry. *Royal Society Open Science*, *3*(1), 150424. https://doi.org/10.1098/rsos.150424

El-Sayed, M. A., & Abdel-Latif, M. A. (2022). Iris recognition approach for identity verification with DWT and multiclass SVM. *PeerJ Computer Science*, *8*, e919. https://doi.org/10.7717/peerj-cs.919

El-Sofany, H., Bouallegue, B., & El-Latif, Y. M. A. (2024). A proposed biometric authentication hybrid approach using Iris recognition for improving cloud security. *Heliyon*, *10*(16), e36390. https://doi.org/10.1016/j.heliyon.2024.e36390

Fathee, H., & Sahmoud, S. (2021). Iris segmentation in uncooperative and unconstrained environments: State-of-the-art, datasets and future research directions. *Digital Signal Processing*, *118*, 103244. https://doi.org/10.1016/j.dsp.2021.103244

Gautam, S., Ahlawat, S., & Mittal, P. (2022). Binary and Multi-class Classification of Brain Tumors using MRI Images. *International Journal of Experimental Research and Review*, 29, 1–9. https://doi.org/10.52756/ijerr.2022.v29.001

Hariharan, G., & Kannan, K. (2014). Review of wavelet methods for the solution of reaction–diffusion problems in science and engineering. *Applied Mathematical Modelling*, *38*(3), 799–813. https://doi.org/10.1016/j.apm.2013.08.003

Hosseinzadeh, M. (2020). Robust control applications in biomedical engineering: Control of depth of hypnosis. In *Elsevier eBooks,* pp. 89–125. https://doi.org/10.1016/b978-0-12-817461-6.00004-4

Illingworth, J., & Kittler, J. (1987). The adaptive Hough transform. *IEEE Transactions on Pattern Analysis and Machine Intelligence*, *PAMI-9*(5), 690–698. https://doi.org/10.1109/tpami.1987.4767964

Jamaludin, S., Zainal, N., & Zaki, W. M. D. W. (2020). Deblurring of noisy iris images in iris recognition. *Bulletin of Electrical Engineering and Informatics*, *10*(1), 156–159. https://doi.org/10.11591/eei.v10i1.2467

Jensen, A., & La Cour-Harbo, A. (2001). Ripples in Mathematics. In *Springer eBooks*. https://doi.org/10.1007/978-3-642-56702-5

Kumar, K. K., Bharadwaj, R. M., & Sujana, S (2021). Iris recognition based on Gabor and Deep Convolutional Networks. In *Proceedings of the International Conference on Communication, Control and Information Sciences (ICCISc 2021)*. https://doi.org/10.1109/iccisc52257.2021.9484905

Larsson, M., Duffy, D. L., Zhu, G., Liu, J. Z., Macgregor, S., McRae, A. F., Wright, M. J., Sturm, R. A., Mackey, D. A., Montgomery, G. W., Martin, N. G., & Medland, S. E. (2011). GWAS Findings for Human Iris Patterns: Associations with Variants in Genes that Influence Normal Neuronal Pattern Development. *The American Journal of Human Genetics*, *89*(2), 334–343. https://doi.org/10.1016/j.ajhg.2011.07.011

Lindfield, G., & Penny, J. (2018). Analyzing data using discrete transforms. In *Elsevier eBooks* (pp. 383–431). https://doi.org/10.1016/b978-0-12-812256-3.00017-8

Madanan, M., Gunasekaran, S. S., & Mahmoud, M. A. (2023). A Comparative Analysis of Machine Learning and Deep Learning Algorithms for Image Classification. In *Proceedings of the International Conference on Contemporary Computing and Informatics, IC3I 2023*, 2436–2439. https://doi.org/10.1109/IC3I59117.2023.10398030

Nazmdeh, V., Mortazavi, S., Tajeddin, D., Nazmdeh, H., & Asem, M. M. (2019). Iris recognition; From classic to modern approaches. In *Proceedings of the IEEE 9th Annual Computing and Communication Workshop and Conference, CCWC 2019*, pp. 981–988. https://doi.org/10.1109/CCWC.2019.8666516

Proença, H., & Alexandre, L. A. (2005). UBIRIS: A Noisy Iris Image database. In *Lecture Notes in Computer Science* (pp. 970–977). https://doi.org/10.1007/11553595_119

Rittig, M., Lütjen-Drecoll, E., Rauterberg, J., Jander, R., & Mollenhauer, J. (1990). Type-VI collagen in the human iris and ciliary body. *Cell and Tissue Research*, *259*(2), 305–312. https://doi.org/10.1007/BF00318453

Roy, D. A., & Soni, U. S. (2016). IRIS segmentation using Daughman's method. In *Proceedings of the International Conference on Electrical, Electronics, and Optimization Techniques, ICEEOT 2016*, pp. 2668–2676. https://doi.org/10.1109/ICEEOT.2016.7755178

Sesmero, M. P., Iglesias, J. A., Magán, E., Ledezma, A., & Sanchis, A. (2021). Impact of the learners diversity and combination method on the generation of heterogeneous classifier ensembles. *Applied Soft Computing*, *111*, 107689. https://doi.org/10.1016/j.asoc.2021.107689

Shen, B., Xu, Y., Lu, G., & Zhang, D. (2007). Detecting iris lacunae based on Gaussian filter. In *Proceedings of the 3rd International Conference on Intelligent Information Hiding and Multimedia Signal Processing, IIHMSP 2007*, pp. 233–236. https://doi.org/10.1109/IIHMSP.2007.4457533

Shen, L., Bai, L., & Fairhurst, M. (2006). Gabor wavelets and General Discriminant Analysis for face identification and verification. *Image and Vision Computing*, *25*(5), 553–563. https://doi.org/10.1016/j.imavis.2006.05.002

Thakkar, S., & Patel, C. (2020). Iris Recognition Supported best Gabor Filters and Deep learning CNN Options. In *Proceedings of the International Conference on Industry 4.0 Technology, I4Tech 2020*, pp. 167–170. https://doi.org/10.1109/I4TECH48345.2020.9102681

Treuting, P. M., Wong, R., Tu, D. C., & Phan, I. (2012). Special Senses. In *Elsevier eBooks* (pp. 395–418). https://doi.org/10.1016/b978-0-12-381361-9.00021-4

Vacca, J. (2007). Biometric Technologies and Verification Systems. Elsevier, eBook ISBN: 9780080488394.

Vishwakarma, N., & Patel, V. (2019). Biometric iris recognition using sobel edge detection for secured authentication. In *Proceedings of the 2nd International Conference on Intelligent Communication and Computational Techniques, ICCT 2019*, pp. 119–123. https://doi.org/10.1109/ICCT46177.2019.8969040

Wei, D., Rajashekar, U., & Bovik, A. C. (2005). Wavelet denoising for image enhancement. In *Elsevier eBooks* (pp. 157–165). https://doi.org/10.1016/b978-012119792-6/50073-5

Xu, W., Liang, Y., Chen, W., & Wang, F. (2019). Recent advances of stretched Gaussian distribution underlying Hausdorff fractal distance and its applications in fitting stretched Gaussian noise. *Physica a Statistical Mechanics and Its Applications*, *539*, 122996. https://doi.org/10.1016/j.physa.2019.122996